2024 IEEE/RSJ International Conference on Intelligent Robots and Systems (IROS)
October 14-18, 2024. Abu Dhabi, UAE

Error-State Kalman Filter based Visual-Inertial Odometry Using Orientation Measurement on Unit Quaternion Group

Chao-Wei Chang and Feng-Li Lian

***Abstract*— The inaccessibility of data from standard sensor suites on closed-platform unmanned aerial vehicles (UAVs) has been a hindrance to developing a compatible visual-inertial odometry (VIO). Despite the advance of recent VIO research, these works often emphasize fusing detailed sensor models with available sensor data at relatively high frequencies. To address this issue, in this paper, we derive an innovation signal for an orientation measurement model on the unit quaternion group $\mathbb{S}^3$ based on the error-state Kalman filter (ESKF) framework. Leveraging the error-state formulation, the innovation signal directly exploits the geometric error representation on $\mathbb{S}^3$ instead of treating unit quaternions as $\mathbb{R}^4$ vectors. Flight experiments on a small commercial UAV (Fig. 1) have been carried out to compare the performance of the proposed ESKF with quaternion measurements on $\mathbb{S}^3$ (ESKF-Q) against the original ESKF framework. Experimental results demonstrate that while both representations of unit quaternion measurements in ESKF framework improve orientation estimates with unperturbed orientation measurement model, only the proposed ESKF-Q exhibits convergent state estimates in the presence of uncertainties in the orientation measurement model.**

I. Introduction

Reliable state estimation is essential for developing applications for the mobile robot. For unmanned aerial vehicles (UAVs), the maneuverability and stability mostly rely on the robustness of the state estimation. Contrary to popular aerial platforms (Ardupilot and PX4), where state estimation is programmed onboard with standard sensor suites at a higher frequency, programming on closed-platforms UAVs such as DJI Ryze Tello, a small commercial quadrotor, is not a common practice. Alternatively, state estimation of these closed-platform UAVs could be developed offboard, though the difficulty arises from only preprocessed sensor data available at a relatively slow rate via decoding packets. While state estimation aided by external facilities such as GPS, fiducial markers, and motion capture systems could achieve up to millimeter-level precision for UAVs, these measurements might not be available in a general scenario for tasks such as autonomous navigation and autonomous aerial filming. Hence, developing a reliable offboard state estimation for closed-platform UAVs is required.

On the other hand, the composition of visual sensors and inertial measurement unit (IMU) for pose estimation as visual-inertial odometry (VIO) have become popular among the research community. Optimization-based VIOs [1]–[3] focus on the construction and optimization of the pose graph consisting of camera and IMU states, which could barely achieve the desired real-time capability owing to the larger state dimension and the joint optimization on the pose graph. Filter-based VIOs [4]–[7] combine the visual measurement with the motion compensated by IMU integration, yet including more camera and landmark states could increase the computational burden and lose the real-time capability of state estimation as well.

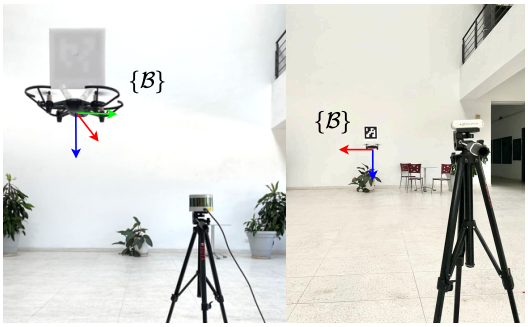

Fig. 1. The experimental setup for evaluation of VIO. A LiDAR screwed on the tripod is used to collect the position of the quadrotor for circle trajectories, and a camera mounted on the tripod is used to measure the pose of the marker on the quadrotor. Both measurements are served as ground truths for odometry evaluation.

On the filter-based state estimation, the fusion of visual sensors and IMU have been well-established via kinematics on the smooth manifold. Multiplicative extended Kalman filter (MEKF) [8], [9] are implemented with the quaternion kinematics, yet measurement models relates to the orientation are discussed on vector space. [10], [11] implement the error-state Kalman filtering (ESKF) [12] based on quaternion kinematics to run the state estimate on PX4 with 100Hz update rate, serving as a low-cost VIO for aerial vehicles.

Filter-based inertial navigation systems considering the symmetry and invariance of Lie group have attracted more attention in recent years. Invariant extended Kalman filter (IEKF) [13] formulates error systems and observers via the invariance of Lie group structure and performs inertial navigation subject to sensor biases by introducing a two-frame group [14]. [15] proposed a nonlinear observer on a non-invariant matrix Lie group to tackle biased angular velocity and linear acceleration measurements in inertial navigation problems. Equivariant filter (EqF) [16], [17] poses the observer state on the symmetry group for homogeneous systems to mitigate the linearization error of the equivariant system output. Nonetheless, these works showcase their results mostly on matrix Lie groups instead of quaternions, where the nonlinear conversion between matrix Lie groups, say $SO(3) \subset \mathbb{R}^{3\times3}$, and unit quaternion group $\mathbb{S}^3$ could induced unwanted discrepancies in filter update.

In this paper, to develop an offboard reliable state estima-

tion for a closed-platform commercial UAV, DJI Ryze Tello, we fuse IMU linear acceleration and angular velocity with noisy linear velocity measurements from its vision positioning system and orientation measurements directly on $\mathbb{S}^3$ from the IMU by exploiting the error-state formulation from the quaternion-based ESKF [10], [11]. In the following content, we coin the proposed ESKF with orientation measurements on $\mathbb{S}^3$ as ESKF-Q. The proposed ESKF-Q serves as a VIO for DJI Ryze Tello with all measurements being preprocessed sensor data sent from Tello available at a lower frequency. The main contributions of this paper are three-fold:

- Derive the innovation signal for an orientation measurement model embedded on the unit quaternion group $\mathbb{S}^3$ using the ESKF framework [11] by exploiting the error-state formulation and the geometric error representation.
- Compare the VIO performance of ESKF-Q and the original ESKF framework with and without quaternion measurements on $\mathbb{R}^4$ against stand-alone space-fixed position measurements from a LiDAR and pose measurements from a camera using fiducial markers on the closed-platform UAV.
- Demonstrate the convergent state estimates of ESKF-Q subject to uncertainties on the proposed orientation measurement model.

The rest of this paper is organized as follows. Section II provides a detailed derivation of ESKF-Q based on the ESKF framework and the orientation measurement model on $\mathbb{S}^3$. Section III introduces the setup for experiments and compares the performances of ESKF with and without orientation measurement model on $\mathbb{R}^4$ and our proposed ESKF-Q. Finally, conclusions are given in Section IV

II. Filter Framework

In this section, we present our proposed ESKF-Q, the ESKF framework [11] combined with the innovation signal for unit quaternions.

A. State Definition and Coordinate System

Our proposed ESKF-Q aims at estimating the true-state $\mathbf{x}_t$ of IMU defined by

$$\mathbf{x}_t = \begin{bmatrix} \mathbf{p}_t^{\mathcal{I}} & \dot{\mathbf{p}}_t^{\mathcal{I}} & \mathbf{q}_t^{\mathcal{B}} & \mathbf{a}_{bt}^{\mathcal{B}} & \boldsymbol{\omega}_{bt}^{\mathcal{B}} \end{bmatrix}^\top,$$

where $\mathbf{p}_t^{\mathcal{I}},\ \dot{\mathbf{p}}_t^{\mathcal{I}} \in \mathbb{R}^3$ denote the position and velocity of $\{\mathcal{B}\}$ expressed in the space-fixed inertial frame $\{\mathcal{I}\}$. $\mathbf{q}_t^{\mathcal{B}} \in \mathbb{S}^3$ is the unit quaternion with the Hamiltonian convention, as in [11], representing the rotation from $\{\mathcal{B}\}$ to $\{\mathcal{I}\}$. $\mathbf{a}_{bt}^{\mathcal{B}},\ \boldsymbol{\omega}_{bt}^{\mathcal{B}} \in \mathbb{R}^3$ are IMU acceleration and angular velocity biases.

Following the ESKF framework [11], [10], we define the true-state $\mathbf{x}_t$ as the *composition* of the nominal-state $\mathbf{x}$ and the error-state $\delta\mathbf{x}$ in our proposed ESKF-Q as follows,

$$\begin{aligned} \mathbf{x}_t &= \mathbf{x} \oplus \delta\mathbf{x} \\ \mathbf{x} &= \begin{bmatrix} \mathbf{p}^{\mathcal{I}} & \dot{\mathbf{p}}^{\mathcal{I}} & \mathbf{q}^{\mathcal{B}} & \mathbf{a}_b^{\mathcal{B}} & \boldsymbol{\omega}_b^{\mathcal{B}} \end{bmatrix}^\top \\ \delta\mathbf{x} &= \begin{bmatrix} \delta\mathbf{p}^{\mathcal{I}} & \delta\dot{\mathbf{p}}^{\mathcal{I}} & \delta\boldsymbol{\theta}_L & \delta\mathbf{a}_b^{\mathcal{B}} & \delta\boldsymbol{\omega}_b^{\mathcal{B}} \end{bmatrix}^\top, \end{aligned}$$

where $\oplus : (\mathbb{R}^6 \times \mathbb{S}^3 \times \mathbb{R}^6) \times (\mathbb{R}^{15}) \to (\mathbb{R}^6 \times \mathbb{S}^3 \times \mathbb{R}^6)$ includes the exponential mapping, composition for the orientation, and the vector addition. Let $\otimes : \mathbb{S}^3 \times \mathbb{S}^3 \to \mathbb{S}^3$ denote the multiplication for unit quaternion group and $\delta\mathbf{q} \in \mathbb{S}^3$ be the error quaternion. Then

$$\delta\mathbf{q} = \mathbf{q}\{\delta\boldsymbol{\theta}\} \triangleq \mathrm{Exp}\Big(\delta\boldsymbol{\theta}\Big) = \begin{bmatrix} \cos\frac{\|\delta\boldsymbol{\theta}\|}{2} \\ \frac{\delta\boldsymbol{\theta}}{\|\delta\boldsymbol{\theta}\|}\sin\frac{\|\delta\boldsymbol{\theta}\|}{2} \end{bmatrix} \tag{1}$$

$$\mathbf{q}_t^{\mathcal{B}} = \mathbf{q}^{\mathcal{B}} \otimes \delta\mathbf{q}_L = \delta\mathbf{q}_G \otimes \mathbf{q}^{\mathcal{B}}, \tag{2}$$

where $\mathrm{Exp}(\cdot) : \mathbb{R}^3 \to \mathbb{S}^3$ maps a rotation vector in $\mathbb{R}^3$ to the unit quaternion group $\mathbb{S}^3$ and sub-scripts $G,\ L$ of error quaternions denote the global (left-hand-side) and local (right-hand-side) representation of the error quaternion respectively.

Assumption 1. According to ESKF framework [10]–[12], second-order products of the error-state $\delta\mathbf{x}$ are negligible owing to its small magnitude.

From Assumption 1, linearization in (1) allows the minimal representation of an error quaternion $\delta\mathbf{q}^\top \approx \begin{bmatrix} 1 & \frac{1}{2}\delta\boldsymbol{\theta}^\top \end{bmatrix}$.

B. Sensor and Measurement Model

In the proposed ESKF-Q, we adopt the IMU model in [10], [11] as

$$\begin{aligned} \mathbf{a}_m^{\mathcal{B}} &= \mathrm{R}_{\mathcal{I}}^{\mathcal{B}}\{\mathbf{q}_t^{\mathcal{B}}\}\Big(\mathbf{a}_t^{\mathcal{I}} - \mathbf{g}^{\mathcal{I}}\Big) + \mathbf{a}_{bt}^{\mathcal{B}} + \mathbf{a}_n^{\mathcal{B}} \\ \boldsymbol{\omega}_m^{\mathcal{B}} &= \boldsymbol{\omega}_t^{\mathcal{B}} + \boldsymbol{\omega}_{bt}^{\mathcal{B}} + \boldsymbol{\omega}_n^{\mathcal{B}}, \end{aligned}$$

where $\mathrm{R}\{\mathbf{q}\} \in SO(3)$ denotes the rotation matrix mapped from the unit quaternion $\mathbf{q}$ and $\mathbf{g}^{\mathcal{I}} \in \mathbb{R}^3$ is the gravitational vector expressed in $\{\mathcal{I}\}$. $\mathbf{a}_n^{\mathcal{B}},\ \boldsymbol{\omega}_n^{\mathcal{B}}$ are additive white noises for the IMU.

To compare ESKF performance with innovation signal defined on $\mathbb{S}^3$ and $\mathbb{R}^4$, we first consider a general orientation measurement model on $\mathbb{S}^3$ as

$$\mathbf{h}_o(\mathbf{x}_t) = \mathbf{q}_0 \otimes \mathbf{q}_t^{\mathcal{B}},\ \boldsymbol{\nu}_o \sim \mathcal{N}(\mathbf{0}, \mathrm{N}_o) \in \mathbb{R}^3 \tag{3}$$

$$\mathbf{y}_o = \mathbf{h}_o(\mathbf{x}_t) \otimes \mathbf{q}_n\{\boldsymbol{\nu}_o\} \in \mathbb{S}^3, \tag{4}$$

where $\mathbf{q}_0 \in \mathbb{S}^3$ denotes a constant offset orientation measured during the filter initialization. Using (3), the orientation measurement model on $\mathbb{R}^4$ could be written as

$$\mathbf{h}_{o,v}(\mathbf{x}_t) = [\mathbf{q}_0]_L \mathbf{q}_t^{\mathcal{B}},\ \mathbf{q}_{n,v} \sim \mathcal{N}(\mathbf{0}, \mathrm{N}_{o,v}) \in \mathbb{R}^4 \tag{5}$$

$$\mathbf{y}_{o,v} = \mathbf{h}_{o,v}(\mathbf{x}_t) + \mathbf{q}_{n,v} \in \mathbb{R}^4, \tag{6}$$

where $[\cdot]_L : \mathbb{S}^3 \to \mathbb{R}^4$ maps a quaternion product on left-hand-side to a left-multiply matrix in $\mathbb{R}^4$ [11].

Assumption 2. $\boldsymbol{\nu}_o$ is assumed to be a small-magnitude white noise rotation vector, and $\mathbf{q}_{o,v}$ is an additive white noise. We also assume that $\mathbb{E}[\delta\mathbf{x}\boldsymbol{\nu}_o^\top] = \mathbb{E}[\delta\mathbf{x}\mathbf{q}_{n,v}^\top] = 0$.

C. State Propagation

We directly adopt discrete-time equations of the state propagation from [10] and [11] in our ESKF-Q due to the same definition of states except for the constant gravitational vector $\mathbf{g}^{\mathcal{I}}$. The state propagation of the nominal-state and the error-state are given as

$$\mathbf{x}(k+1) = \mathbf{f}(\mathbf{x}(k), \mathbf{u}_m(k))$$
$$\delta\mathbf{x}(k+1) = \mathrm{F}_{\mathbf{x}}\Big(\mathbf{x}(k),\ \mathbf{u}_m(k)\Big)\delta\mathbf{x}(k) + \mathrm{F}_{\mathbf{i}}\mathbf{i}(k),$$

where we follow the definition and settings in [10] and [11] to construct the IMU input $\mathbf{u}_m(k) = \begin{bmatrix}\mathbf{a}_m^{\mathcal{B}\top}(k) & \boldsymbol{\omega}_m^{\mathcal{B}\top}(k)\end{bmatrix}^\top$ and the random impulse $\mathbf{i}(k) = \begin{bmatrix}\mathbf{v_i}^{\mathcal{I}\top}(k) & \boldsymbol{\theta_i}^\top(k) & \mathbf{a_i}^{\mathcal{B}\top}(k) & \boldsymbol{\omega_i}^{\mathcal{B}\top}(k)\end{bmatrix}^\top$. The prior prediction of the error-state and its covariance is calculated as

$$\hat{\delta\mathbf{x}}^-(k+1) = \mathrm{F}_{\mathbf{x}}(\mathbf{x}(k),\ \mathbf{u}_m(k))\hat{\delta\mathbf{x}}^-(k) \tag{7}$$
$$\mathrm{P}^-(k+1) = \mathrm{F}_{\mathbf{x}}\mathrm{P}(k)\mathrm{F}_{\mathbf{x}}^\top + \mathrm{F}_{\mathbf{i}}\mathrm{Q}_{\mathbf{i}}\mathrm{F}_{\mathbf{i}}^\top, \tag{8}$$

where $\mathrm{Q}_{\mathbf{i}}$ is the covariance matrix of Gaussian random impulse $\mathbf{i}(k)$. $\hat{\delta\mathbf{x}}^-$ denotes the prior estimate of the error-state $\delta\mathbf{x}$, $\mathrm{P}^-(k)$ is the prior error-state covariance, and $\mathrm{P}(k)$ is the posterior error-state covariance.

Assumption 3. Assume the nominal-state coincides with the true-state initially, i.e. we have the error-state estimate with zero initial condition $\hat{\delta\mathbf{x}}^-(k=0) = \mathbf{0}$ [11].

Since we adopt the same reset process (Section II-E) as Section 6.3 in [11], (7) always remains zero according to Assumption 3.

D. Filter Update

For measurements on the vector space $\mathbf{y}_\mu = \mathbf{h}_\mu(\mathbf{x}_t) + \mathbf{n}_\mu$, ESKF-Q adopts same update equations as ESKF [11],

$$\mathrm{K} = \mathrm{P}^-\mathrm{H}_\mu^\top(\mathrm{H}_\mu\mathrm{P}^-\mathrm{H}_\mu^\top + \mathrm{N}_\mu)^{-1},\ \hat{\delta\mathbf{x}} = \mathrm{K}(\mathbf{y}_\mu - \mathbf{h}_\mu(\mathbf{x})) \tag{9}$$

$$\mathrm{P} = \Big(\mathrm{I} - \mathrm{K}\mathrm{H}_\mu\Big)\mathrm{P}^-\Big(\mathrm{I} - \mathrm{K}\mathrm{H}_\mu\Big)^\top + \mathrm{K}\mathrm{N}_\mu\mathrm{K}^\top \tag{10}$$

with time index k dropped. H_μ is the Jacobian matrix of the measurement function $\mathbf{h}_\mu$ with regard to the error-state. For the orientation measurement model on $\mathbb{R}^4$ in (5), the Jacobian matrix is calculated as

$$\mathrm{H}_o = \mathrm{H}_{o,\mathbf{x}}\mathrm{X}_{\delta\mathbf{x}},\ \mathrm{H}_{o,\mathbf{x}} = \begin{bmatrix}0_{4\times6} & [\mathbf{q}_0]_L & 0_{4\times6}\end{bmatrix}, \tag{11}$$

where $\mathrm{X}_{\delta\mathbf{x}}$ follows the same definition in [11].

However, for measurements on the unit quaternion group $\mathbb{S}^3$ as (4), the innovation signal could not be implemented with (9). Thus, in our proposed ESKF-Q, we define the innovation signal to exploit the error-state property with the measurement equation (4) and correpsonding noise properties (Assumption 2).

Definition 1. Define the innovation signal on $\mathbb{S}^3$ as

$$\boldsymbol{\alpha}(k) \triangleq \mathrm{Log}\Big(\mathbf{h}_o^*(\mathbf{x}(k)) \otimes \mathbf{y}_o(k)\Big) \in \mathbb{R}^3, \tag{12}$$

where $\mathrm{Log}(\cdot) : \mathbb{S}^3 \to \mathbb{R}^3$ is the inverse mapping of $\mathrm{Exp}(\cdot)$. Expand (12) with (3), (4), and (2),

$$\begin{aligned}\boldsymbol{\alpha}(k) &= \mathrm{Log}\Big(\mathbf{h}_o^*(\mathbf{x}(k)) \otimes \mathbf{h}_o(\mathbf{x}_t(k)) \otimes \mathbf{q}_n\Big)\\ &= \mathrm{Log}\Big(\mathbf{q}^{\mathcal{B}^*}(k) \otimes \mathbf{q}_t^{\mathcal{B}}(k) \otimes \mathbf{q}_n\{\boldsymbol{\nu}_o\}\Big)\\ &= \mathrm{Log}\Big(\delta\mathbf{q}_L(k) \otimes \mathrm{Exp}\Big(\boldsymbol{\nu}_o\Big)\Big),\ \delta\mathbf{q}_L = \mathrm{Exp}\Big(\delta\boldsymbol{\theta}_L\Big)\\ &\approx \delta\boldsymbol{\theta}_L(k) + \mathrm{J}_r^{-1}(\delta\boldsymbol{\theta}_L(k))\boldsymbol{\nu}_o,\end{aligned} \tag{13}$$

where $(\cdot)^*$ denotes the quaternion conjugation and the inverse of right Jacobian on $\mathbb{S}^3$ [11], [18] is

$$\mathrm{J}_r^{-1}(\phi\mathbf{u}) = \mathrm{I} + \frac{1}{2}[\phi\mathbf{u}]_\times + \Big(\frac{1}{\phi^2} - \frac{1+\cos\phi}{2\phi\sin\phi}\Big)[\phi\mathbf{u}]_\times^2. \tag{14}$$

Owing to Assumption 2, the first-order approximation for the logarithm in (13) holds by the linearization around the local representation of the error rotation vector $\delta\boldsymbol{\theta}_L$. Derive the posterior estimate of the error-state as

$$\begin{aligned}\hat{\delta\mathbf{x}}(k) &= \mathrm{K}(k)\boldsymbol{\alpha}(k)\\ \hat{\delta\mathbf{x}}(k) &\approx \mathrm{K}(k)\mathrm{C}_{\delta\boldsymbol{\theta}}\delta\mathbf{x}(k) + \mathrm{K}(k)\mathrm{J}_r^{-1}(\delta\boldsymbol{\theta}_L(k))\boldsymbol{\nu}_o,\end{aligned} \tag{15}$$

where $\mathrm{C}_{\delta\boldsymbol{\theta}} = \begin{bmatrix}0_{3\times6} & \mathrm{I}_3 & 0_{3\times6}\end{bmatrix}$ is a constant selection matrix mapping $\delta\mathbf{x}$ to $\delta\boldsymbol{\theta}_L$.

To derive the optimal Kalman gain $\mathrm{K}_{opt}(k)$ in the sense of minimizing the trace of the error-state covariance, we write the definition of $\mathrm{P}(k)$ and $\mathrm{P}^-(k)$ in (8) as

$$\mathrm{P}(k) \triangleq \mathrm{Cor}\Big(\delta\mathbf{x}(k) - \hat{\delta\mathbf{x}}(k)\Big) \tag{16}$$
$$\mathrm{P}^-(k) \triangleq \mathrm{Cor}\Big(\delta\mathbf{x}(k) - \hat{\delta\mathbf{x}}^-(k)\Big) = \mathrm{Cor}\Big(\delta\mathbf{x}(k)\Big), \tag{17}$$

where $\mathrm{Cor}(\cdot)$ is the correlation of a stochastic signal. The covariance propagation with our posterior error-state estimate (15) could be derived as follows,

$$\begin{aligned}\delta\mathbf{x}(k) - \hat{\delta\mathbf{x}}(k) \approx &\Big(\mathrm{I} - \mathrm{K}(k)\mathrm{C}_{\delta\boldsymbol{\theta}}\Big)\delta\mathbf{x}(k)\\ &- \mathrm{K}(k)\mathrm{J}_r^{-1}(\delta\boldsymbol{\theta}_L(k))\boldsymbol{\nu}_o\end{aligned} \tag{18}$$

$$\begin{aligned}\mathrm{P}(k) \approx &\ \mathrm{F}_c(k)\mathrm{Cor}\Big(\delta\mathbf{x}(k)\Big)\mathrm{F}_c^\top(k)\\ &+ \mathrm{K}(k)\mathrm{Cor}\Big(\mathrm{J}_r^{-1}(k)\boldsymbol{\nu_o}\Big)\mathrm{K}^\top(k)\end{aligned} \tag{19}$$

$$\mathrm{F}_c(k) \triangleq \Big(\mathrm{I} - \mathrm{K}(k)\mathrm{C}_{\delta\boldsymbol{\theta}}\Big). \tag{20}$$

Simplify (19) with (17), and Assumption 2 and 3 to derive

$$\begin{aligned}\mathrm{P}(k) \approx &\ \mathrm{F}_c(k)\mathrm{P}^-(k)\mathrm{F}_c^\top(k)\\ &+ \mathrm{K}(k)\mathrm{J}_r^{-1}(\hat{\delta\boldsymbol{\theta}}_L(k))\mathrm{N}_o\mathrm{J}_r^{-\top}(\hat{\delta\boldsymbol{\theta}}_L(k))\mathrm{K}^\top(k).\end{aligned} \tag{21}$$

According to the ESKF framework in [11], since the posterior true-state estimate is not yet injected, $\mathbb{E}[\delta\mathbf{x}] = \hat{\delta\mathbf{x}}^- = \mathbf{0}$ and $\mathbb{E}[\mathbf{x}_t] = \mathbf{x}$. Hence, by Assumption 3, (14) could be reduced as

$$\mathrm{J}_r^{-1}(\hat{\delta\boldsymbol{\theta}}_L^-(k)) = \mathrm{J}_r^{-1}\Big(\mathbb{E}[\delta\boldsymbol{\theta}_L^-(k)]\Big) = \mathrm{I}_3, \tag{22}$$

and (21) could be simplified as

$$\mathrm{P}(k) \approx \mathrm{F}_c(k)\mathrm{P}^-(k)\mathrm{F}_c^\top(k) + \mathrm{K}(k)\mathrm{N}_o\mathrm{K}^\top(k), \tag{23}$$

which is similar to (10) with the Jacobian H_μ replaced by $\mathrm{C}_{\delta\boldsymbol{\theta}}$, as reported in [5].

Finally, with the covariance propagation formula in (23), $\mathrm{K}_{opt}(k)$ could be derived as follows,

$$\frac{\partial\mathrm{tr}\Big(\mathrm{P}(k)\Big)}{\partial\mathrm{K}(k)}\Big|_{\mathrm{K}(k)=\mathrm{K}_{opt}(k)} = 0$$
$$\mathrm{K}_{opt}(k) \triangleq \mathrm{P}^-(k)\mathrm{C}_{\delta\boldsymbol{\theta}}^\top\Big(\mathrm{C}_{\delta\boldsymbol{\theta}}\mathrm{P}^-(k)\mathrm{C}_{\delta\boldsymbol{\theta}}^\top + \mathrm{N}_o\Big)^{-1}. \tag{24}$$

E. Injection and Reset

We follow the ESKF framework [11] with the same injection and reset process as

$$\hat{\mathbf{x}}_t(k) = \mathbf{x}(k) \oplus \hat{\delta\mathbf{x}}(k) \tag{25}$$
$$\hat{\delta\mathbf{x}}^{-}(k+1) = \mathbf{0},\ \mathrm{P}^{-}(k+1) = \mathrm{G}(k)\mathrm{P}(k)\mathrm{G}^{\top}(k)$$

with $\mathrm{G}(k)$ being the Jacobian matrix of the reset function $\mathbf{g}(\cdot)$ in Section 6.3 of [11].

III. Experimental Results

We compare the quantitative results on the odometry evaluation task for a commercial quadrotor of the proposed ESKF-Q to the ESKF with and without orientation measurement on $\mathbb{R}^4$ as (5) (ESKF-q4d). Both ESKF, ESKF-Q, and ESKF-q4d are implemented with C++ library `Eigen` and runs on an i7 8-core 16GB RAM laptop with 100Hz.

A. Experiment Setup

a) Commercial Quadrotor

We adopt Ryze Tello , a small quadrotor with size 150 mm×150 mm and weight 87 g, for the odometry evaluation experiment. Communication between our laptop and Tello is addressed via ROS [19] with an unofficial wrapper `tello_driver` [20] for Tello . From `tello_driver`, IMU linear acceleration $\mathbf{a}_m^{\mathcal{B}}$, angular velocity $\boldsymbol{\omega}_m^{\mathcal{B}}$, and orientation measurement in quaternion $\mathbf{q}_m^{\mathcal{B}}$ are available at around 20 Hz, so as the velocity measurement from the vision positioning system of Tello $\mathbf{v}^{\mathcal{O}}$ under a space-fixed frame $\mathcal{O}$. The measurement model of linear velocity $\mathbf{v}^{\mathcal{O}}$ could be derived as

$$\mathbf{h}_{\mathcal{O}}(\mathbf{x}_t) = \mathrm{R}_{\mathcal{I}}^{\mathcal{O}}\dot{\mathbf{p}}_t^{\mathcal{I}},\ \mathbf{n}_{\mathcal{O}} \sim \mathcal{N}(\mathbf{0}, \mathrm{N}_{\mathcal{O}}) \tag{26}$$
$$\mathbf{y}_{\mathcal{O}} = \mathbf{v}^{\mathcal{O}} = \mathbf{h}_{\mathcal{O}}(\mathbf{x}_t) + \mathbf{n}_{\mathcal{O}}. \tag{27}$$

$\mathbf{q}_m^{\mathcal{B}} = \mathbf{y}_o$ in (4) and $\mathbf{q}_m^{\mathcal{B}} = \mathbf{y}_{o,v}$ in (6) with $\mathbf{q}_0 = \mathbf{q}_{\mathcal{I}\to\mathcal{B}_0}$ being the rotation from inertial frame $\{\mathcal{I}\}$ to initial gyrometer frame $\{\mathcal{B}_0\}$. In our proposed ESKF-Q, we adopt both measurements in our filter framework with $\mathbf{v}^{\mathcal{O}}$ updating the filter via (9)-(10) and $\mathbf{q}_m^{\mathcal{B}}$ via (15), (24), and (23).

b) Filter Initialization and Parameters

We adopt the same parameter set and initialization for all three ESKF method. $\sigma_{\omega_n}^2 = 10^{-6}(s^{-2})$, $\sigma_{a_n}^2 = 10^{-4}(m^2s^{-4})$, $\sigma_{\omega_w}^2 = 10^{-8}(s^{-5})$, and $\sigma_{a_w}^2 = 10^{-8}(m^2s^{-5})$, which constructs Q_i in (8) following Section 5.4.2 in [11]. $\mathrm{N}_o = 10^{-6}\mathrm{I}_3$ in (3), $\mathrm{N}_{o,v} = 10^{-6}\mathrm{I}_4$ in (5), and $\mathrm{N}_{\mathcal{O}} = 10^{-6}\mathrm{I}_3$ in (26). We set the inertial frame $\{\mathcal{I}\}$ coincide with $\{\mathcal{O}\}$ so $\mathrm{R}_{\mathcal{I}}^{\mathcal{O}} = \mathrm{I}_3$.

The constant offset rotation $\mathbf{q}_0 = \mathbf{q}_{\mathcal{I}\to\mathcal{B}_0}$ is estimated during the filter initialization by

$$\mathbf{q}_0 = \mathbf{q}_{\mathcal{I}\to\mathcal{B}_0} = \mathbf{q}_m^{\mathcal{B}} \otimes \mathbf{q}_t^{\mathcal{B}*}. \tag{28}$$

We model the uncertainties on the orientation model in (3) and (5) by,

$$\mathbf{q}_{0,pb} = \mathbf{q}_0 \otimes \Delta\mathbf{q}\{\Delta\theta\mathbf{u}\},\ \mathbf{u} \in \mathbb{R}^3,\ \|\mathbf{u}\| = 1, \tag{29}$$

where $\mathbf{u}$ is the axis vector of $\mathbf{q}_0$. The perturbed measurement model adopts (29) instead of (28) as the constant offset rotation. Such fixed uncertainty could happen in case the drone is moved after the filter initialization or the transformation between $\{\mathcal{I}\}$ and $\{\mathcal{B}_0\}$ is not modeled correctly in prior.

c) LiDAR and Marker Measurement

To provide a space-fixed measurement for the position of Tello, a Velodyne's Puck LiDAR (VLP-16) screwed on a tripod is mounted on the floor at the height of 1m. To extract the position of Tello from the point cloud data $\mathbf{p}_{lidar,i}$ for the i-th frame, we filter out the background points by the distance threshold $d_{thr} \in \mathbb{R}$ and the bounding box $B \subset \mathbb{R}^3$, and then calculate the mean position of the points $\mathbf{p}_{lidar,i}$. Let the desired set of points denote as $\mathcal{Q}_i = \{\mathbf{p} \in \mathcal{P}_i |\ \|\mathbf{p}\| < d_{thr}, \mathbf{p} \in B\}$ with $\mathcal{P}_i$ being the set of points received from VLP-16. The mean position of desired points is

$$\mathbf{p}_{lidar,i} = \sum_{\mathbf{p}_j \in \mathcal{Q}_i} \mathbf{p}_j / |\mathcal{Q}_i|. \tag{30}$$

To provide a space-fixed pose measurement of Tello, we stick a thin foamboard on Tello with ArUco markers attached on it, and relative poses from marker to camera are extracted via `OpenCV` library. The measured pose of Tello is given by

$$\mathbf{q}_C^{\mathcal{B}} = \mathbf{q}_{C\to\mathcal{I}} \otimes \mathbf{q}_{M\to C} \otimes \mathbf{q}_{\mathcal{B}\to M} \tag{31}$$
$$\mathbf{p}_C^{\mathcal{I}} = \mathbf{p}_{\mathcal{I}\to C}^{\mathcal{I}} + \mathrm{R}_C^{\mathcal{I}}\mathbf{p}_{C\to M}^{C}, \tag{32}$$

where $\{M\}$ is the marker frame on Tello and $\{C\}$ is the stand-alone camera frame. $\mathbf{q}_{M\to C}$, $\mathbf{p}_{C\to M}^{C}$ are measured from markers and $\mathbf{q}_{C\to\mathcal{I}}$, $\mathbf{q}_{\mathcal{B}\to M}$, $\mathbf{p}_{\mathcal{I}\to C}^{\mathcal{I}}$, $\mathrm{R}_C^{\mathcal{I}}$ are known parameters.

B. Performance Comparison with Unperturbed Orientation Measurement Model

Experimental results of three square trajectories (Sq-1, Sq-2, and Sq-3) and three circular trajectories (Cir-1, Cir-2, and Cir-3) carried out via Tello are summarized in this subsection (Table I). The unit of metrics regarding position, orientation, and experiment time are in meters, radians, and seconds respectively. We compute the error between unit quaternions as the geometric error on $\mathbb{S}^3$, and the error between vectors simply as the 2-norm. With position references from (30) and (32) and orientation references from (31), the position and orientation errors listed in Table I are computed by

$$e_p = \begin{cases} \|\hat{\mathbf{p}}_t - \mathbf{p}_{lidar}\|_2, & \text{Cir-i},\ i = 1,2,3 \\ \|\hat{\mathbf{p}}_t - \mathbf{p}_C^{\mathcal{B}}\|_2, & \text{Sq-i},\ i = 1,2,3 \end{cases} \tag{33}$$

$$\theta_{err} = \|\mathrm{Log}\Big(\hat{\mathbf{q}}_t^* \otimes \mathbf{q}_C^{\mathcal{B}}\Big)\|_2,\ \text{Sq-i},\ i = 1,2,3, \tag{34}$$

where $\hat{\cdot}$ denotes the true-state estimate from (25). Considering the visibility of markers for circular trajectories, the pose measurement is not provided by markers and thus only position measurement from LiDAR is available.

From Table I, both ESKF-Q and ESKF-q4d have significant improvement in terms of the orientation estimation as compared to ESKF, which even undergoes a large orientation root-mean-square errors (RMSEs) of 3.055 in flight Sq-2. The difference in position estimates between three methods is apparently smaller, since Tello have provided linear velocity measurement under a space-fixed frame (26) such that the

TABLE I

POSE ESTIMATION COMPARISON BETWEEN ESKF [11], ESKF-Q4D [11], AND ESKF-Q. OUTPERFORMING RESULTS ARE MARKED IN BOLD.

Flight	ESKF [11]				ESKF-q4d [11]				ESKF-Q			
	Pos. RMSE	Pos. err. max	Orient. RMSE	Orient. err. max	Pos. RMSE	Pos. err. max	Orient. RMSE	Orient. err. max	Pos. RMSE	Pos. err. max	Orient. RMSE	Orient. err. max
Sq-1	0.472	1.033	0.448	1.204	0.471	1.029	**0.312**	**0.908**	0.468	1.029	**0.312**	**0.911**
Sq-2	0.609	0.976	3.055	6.134	0.613	0.970	**0.327**	**0.969**	0.613	0.973	**0.328**	**0.970**
Sq-3	1.214	1.610	0.710	1.197	1.214	1.612	**0.322**	**0.749**	1.215	1.613	**0.321**	**0.742**
Cir-1	0.299	0.504	-	-	0.306	0.512	-	-	0.306	0.516	-	-
Cir-2	0.529	0.763	-	-	0.533	0.763	-	-	0.536	0.769	-	-
Cir-3	0.428	0.578	-	-	0.427	0.577	-	-	0.427	0.579	-	-

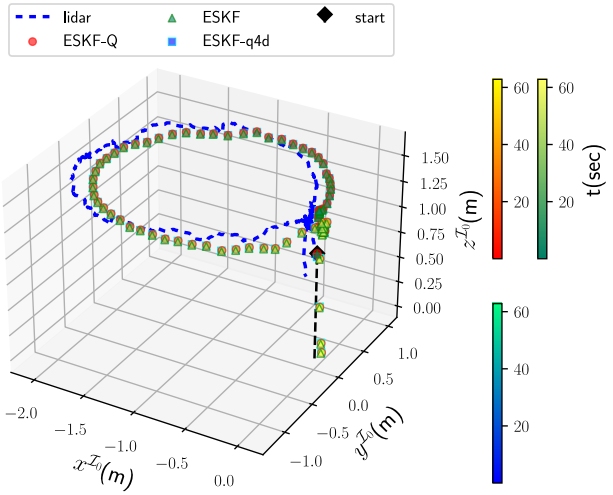

Fig. 2. The visualization of 3D trajectories from VLP-16 measurement, ESKF-Q, ESKF, and ESKF-q4d for flight Cir-1 in the inertial frame $\{\mathcal{I}\}$. Colorbars indicate the time stamps of trajectory points from compared methods.

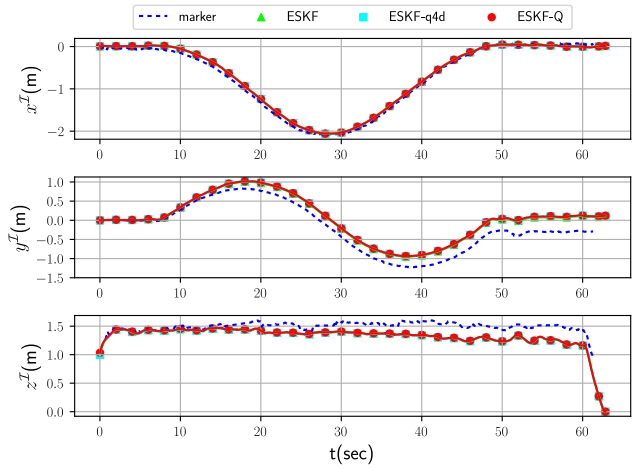

Fig. 3. Comparison of estimated position from VLP-16 measurement, ESKF-Q, ESKF, and ESKF-q4d for flight Cir-1 in the inertial frame $\{\mathcal{I}\}$.

error of the estimated orientation would not propagate to the estimate of $\mathbf{p}^{\mathcal{I}}$, $\dot{\mathbf{p}}^{\mathcal{I}}$ drastically.

Figures 2 to 4 illustrate the discrepancy of estimated states between ESKF and ESKF-Q for flight Cir-1 in detail. Fig. 2 and Fig. 3 reveal that the odometry estimated by all three methods possess apparent drifts in both the y-axis and z-axis of $\{\mathcal{I}\}$, and Fig. 4 indicates that ESKF-Q and ESKF-q4d estimate small magnitude of bias terms from the noisy IMU linear acceleration and angular velocity, while ESKF calculates obvious larger bias terms to compensate the estimated circular motion in Fig. 2 and Fig. 3.

C. Performance Comparison with Perturbed Orientation Measurement Model

Experimental results of applying the perturbed constant offset rotation (29) to the measurement model on $\mathbb{S}^3$ (3) and the measurement model on $\mathbb{R}^4$ (5) for state estimation of flight Sq-1 and Cir-1 is shown in Fig. 5 and Fig. 6. As the proposed ESKF-Q adopts the geometric error representation on $\mathbb{S}^3$ in Definition 1, the orientation uncertainties would be measured with convergent state estimates. In contrast, vector subtraction on $\mathbb{R}^4$ (9) adopted by ESKF-q4d is not valid for larger perturbation angle $\Delta\theta$, in turns causing pose estimates diverge. Note that ESKF does not consider the orientation measurement model, and thus not affected by $\mathbf{q}_0$.

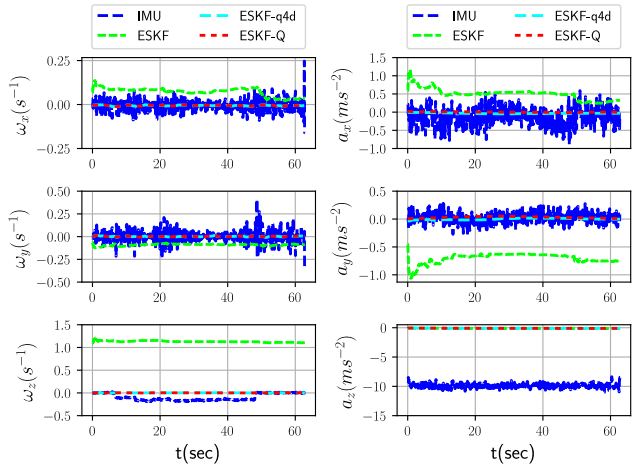

Fig. 4. Comparison of estimated bias from ESKF, ESKF-Q, and ESKF-q4d with measured values of linear acceleration and angular velocity from IMU for flight Cir-1.

IV. CONCLUSION

In this paper, we derive the innovation signal (Definition 1) for an orientation measurement model on $\mathbb{S}^3$ explicitly considering the geometric error representation on $\mathbb{S}^3$ and the quaternion-based ESKF framework [10], [11]. We coin the quaternion-based ESKF framework with such innova-

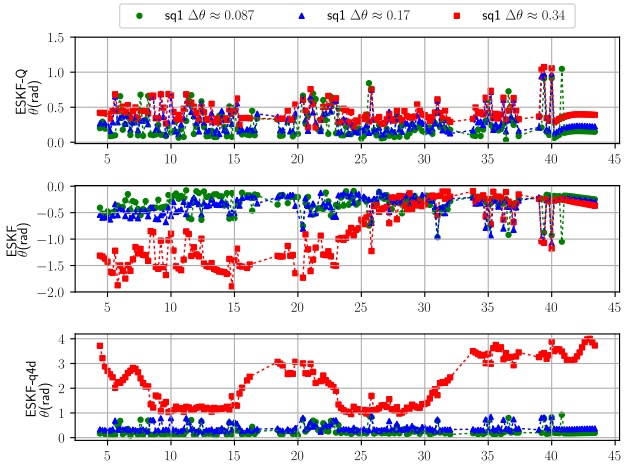

Fig. 5. Orientation error profiles of ESKF, ESKF-Q, and ESKF-q4d for flight Sq-1 with differnet magnitude of perturbation angle. All x-axis ticks are time stamps in second.

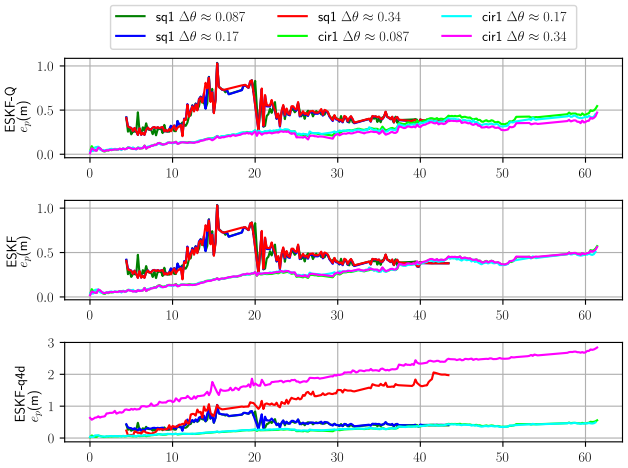

Fig. 6. Position error profiles of ESKF, ESKF-Q, and ESKF-q4d for flight Cir-1 with different magnitude of perturbation angle. All x-axis ticks are time stamps in second.

tion signal as ESKF-Q and compare the state estimation performance with original ESKF with and without quaternion measurements as $\mathbb{R}^4$ vectors (ESKF-q4d and ESKF, respectively). Quantitative comparison of different odometry estimation tasks using a closed-platform commercial UAV demonstrates an improvement in orientation estimates of using quaternion measurement in both representations with comparable position estimates. Nonetheless, in case of model uncertainties on the orientation measurement, state estimation results of ESKF-q4d diverge owing to the violation of small-angle assumption on the orientation innovation signal using vector subtraction, while the state estimates of ESKF-Q converge closed to the perturbed angle, thanks to the innovation signal using geometric error representation on $\mathbb{S}^3$. We conclude that ESKF-Q provides a better approach for fusing an orientation measurement model on $\mathbb{S}^3$ than ESKF-q4d and ESKF, especially for those offboard state estimation where orientation measurement comes in a lower frequency. Further research could include comparisons of the fusion of orientation measurement and different sensor suits using the proposed ESKF-Q, and the improvement in state propagation of ESKF-Q when sensor packets are lost.

References

[1] S. Shen, N. Michael, and V. Kumar, "Tightly-coupled monocular visual-inertial fusion for autonomous flight of rotorcraft mavs," in *2015 IEEE International Conference on Robotics and Automation (ICRA)*, 2015, pp. 5303–5310.

[2] C. Forster, L. Carlone, F. Dellaert, and D. Scaramuzza, "On-manifold preintegration for real-time visual–inertial odometry," *IEEE Transactions on Robotics*, vol. 33, no. 1, pp. 1–21, 2017.

[3] T. Qin, P. Li, and S. Shen, "Vins-mono: A robust and versatile monocular visual-inertial state estimator," *IEEE Transactions on Robotics*, vol. 34, no. 4, pp. 1004–1020, 2018.

[4] A. I. Mourikis and S. I. Roumeliotis, "A multi-state constraint kalman filter for vision-aided inertial navigation," in *Proceedings 2007 IEEE International Conference on Robotics and Automation*, 2007, pp. 3565–3572.

[5] M. Bloesch, M. Burri, S. Omari, M. Hutter, and R. Siegwart, "Iterated extended kalman filter based visual-inertial odometry using direct photometric feedback," *The International Journal of Robotics Research*, vol. 36, no. 10, pp. 1053–1072, 2017.

[6] K. Sun, K. Mohta, B. Pfrommer, *et al.*, "Robust stereo visual inertial odometry for fast autonomous flight," *IEEE Robotics and Automation Letters*, vol. 3, no. 2, pp. 965–972, 2018.

[7] R. G. Thalagala, O. De Silva, G. K. I. Mann, and R. G. Gosine, "Two key-frame state marginalization for computationally efficient visual inertial navigation," in *2021 European Control Conference (ECC)*, IEEE, pp. 1138–1143.

[8] F. L. Markley, "Attitude error representations for kalman filtering," *Journal of Guidance, Control, and Dynamics*, vol. 26, no. 2, pp. 311–317, Mar. 2003.

[9] R. Zanetti and R. Bishop, "Quaternion estimation and norm constrained kalman filtering," in *AIAA/AAS Astrodynamics Specialist Conference and Exhibit*.

[10] A. Santamaria-Navarro, J. Solà, and J. Andrade-Cetto, "High-frequency mav state estimation using low-cost inertial and optical flow measurement units," in *2015 IEEE/RSJ International Conference on Intelligent Robots and Systems (IROS)*, 2015, pp. 1864–1871.

[11] J. Solà, "Quaternion kinematics for the error-state kalman filter," 2017. arXiv: `1711.02508 [cs.RO]`.

[12] V. Madyastha, V. Ravindra, S. Mallikarjunan, and A. Goyal, "Extended kalman filter vs. error state kalman filter for aircraft attitude estimation," in *AIAA Guidance, Navigation, and Control Conference*, American Institute of Aeronautics and Astronautics, Aug. 8, 2011.

[13] A. Barrau and S. Bonnabel, "The invariant extended kalman filter as a stable observer," *IEEE Transactions on Automatic Control*, vol. 62, no. 4, pp. 1797–1812, 2017.

[14] A. Barrau and S. Bonnabel, "The geometry of navigation problems," *IEEE Transactions on Automatic Control*, vol. 68, no. 2, pp. 689–704, 2023.

[15] M. Wang and A. Tayebi, "Hybrid nonlinear observers for inertial navigation using landmark measurements," *IEEE Transactions on Automatic Control*, vol. 65, no. 12, pp. 5173–5188, 2020.

[16] P. van Goor, T. Hamel, and R. Mahony, "Equivariant filter (eqf)," *IEEE Transactions on Automatic Control*, vol. 68, no. 6, pp. 3501–3512, 2023.

[17] A. Fornasier, Y. Ge, P. van Goor, R. Mahony, and S. Weiss, "Equivariant symmetries for inertial navigation systems," 2023. arXiv: `2309.03765 [cs.RO]`.

[18] G. S. Chirikjian, *Stochastic Models, Information Theory, and Lie Groups, Volume 2: Analytic Methods and Modern Applications* (Applied and Numerical Harmonic Analysis). Boston: Birkhäuser Boston, 2012.

[19] M. Quigley, "ROS: An open-source robot operating system," in *IEEE International Conference on Robotics and Automation*, 2009.

[20] A. Xu. "anqixu/tello_driver." (2018), [Online]. Available: `https://github.com/anqixu/tello_driver/tree/master` (visited on 10/08/2023).